The total neutron cross section of liquid para-hydrogen

1999 J. Phys.: Condens. Matter 11 10229

(http://iopscience.iop.org/0953-8984/11/50/315)

J. Phys.: Condens. Matter **11** (1999) 10229–10242. Printed in the UK PII: S0953-8984(99)05575-7

The total neutron cross section of liquid para-hydrogen

M Celli†, N Rhodes‡, A K Soper‡ and M Zoppi†

† Consiglio Nazionale delle Ricerche, Istituto di Elettronica Quantistica, Via Panciatichi 56/30, I-50127 Firenze, Italy

‡ Rutherford Appleton Laboratory, ISIS Neutron Facility, Chilton, Didcot, Oxon OX11 0QX, UK

Received 28 June 1999, in final form 1 November 1999

Abstract. We have measured, using the pulsed neutron source ISIS, the total neutron cross section of liquid para-hydrogen in the vicinity of the triple point. The experimental results compare only qualitatively with the results of the Young and Koppel theory. However, a much better agreement is found once modifications are included in the model which effectively take into account the intermolecular interactions.

1. Motivation

In the experimental investigations of the microscopic structure of quantum liquids, hydrogen is one of the most interesting cases. In fact, the peculiar behaviour of a quantum liquid can be considered to arise from the delocalization of the particles, due to the spread of its wave packet as measured by the de Broglie thermal wavelength $\Lambda_{DB} = h/(2\pi M k_B T)^{1/2}$ [1]. Here h is Planck's constant, k_B is the Boltzmann constant, M is the particle mass, and T is the temperature. When Λ_{DB} becomes sizable with respect to σ (the hard-core diameter of the particle), quantum diffraction effects start to emerge. However, the particles retain their distinguishability and Boltzmann statistics still applies. In contrast, at very low temperature, when Λ_{DB} becomes comparable with the average interparticle distance, l, the delocalization is such as to allow the occurrence of exchange effects, and quantum statistics begins to play a role. As is known, liquid ^{4}He belongs to the latter category and its microscopic properties are strongly related to the quantum Bose statistics. However, liquid hydrogen is not affected by quantum exchange, and its microscopic properties are only determined by quantum diffraction [2].

Therefore, hydrogen is a very important example for studying the quantum diffraction properties of matter, without having to introduce the complication of quantum statistics, but in a situation where the effects of delocalization are relevant and cannot be simply considered as small perturbations of a substantially classical behaviour. Such an intermediate case is very important because theories and simulation techniques are much more easily implemented in the absence of quantum exchange, when the individual molecules can be modelled as Boltzmann particles [3]. Quantitatively, the situation is depicted in table 1.

Due to the large incoherent neutron scattering cross section of protons, neutron diffraction experiments on hydrogen are extremely difficult. However, the experimental information on the microscopic structure of hydrogen is of fundamental importance. For this reason, we have carried out, recently, a neutron diffraction experiment on liquid hydrogen. The data were good enough (and the instrumental set-up stable enough) for us to obtain the thermodynamic derivatives of the microscopic structure factor [4]. Nonetheless, the analysis

0953-8984/99/5010229+14$30.00

Table 1. Evaluation of quantum effects for common quantum liquids. The subscripts CP and TP refer to the critical point and to the triple point, respectively. For helium, TP indicates the λ-point. Λ_{DB} is the de Broglie wavelength defined in section 1. The parameters σ and l represent the hard-core diameter of the particle and the average interparticle distance, respectively.

System	T_{CP} (K)	T_{TP} (K)	n_{CP} (nm^{-3})	n_{TP} (nm^{-3})	$(\Lambda_{DB}/\sigma)_{CP}$	$(\Lambda_{DB}/\sigma)_{TP}$	$(\Lambda_{DB}/l)_{CP}$	$(\Lambda_{DB}/l)_{TP}$
He	5.20	2.18	10.47	21.99	1.50	2.31	0.84	1.66
H_2	33.19	13.96	9.00	23.06	0.72	1.11	0.44	0.94
D_2	38.34	18.71	10.44	25.99	0.47	0.68	0.31	0.60
Ne	44.4	24.55	14.31	37.2	0.21	0.29	0.14	0.26

of the experimental data was rather difficult and we were unable to obtain reliable results on the structure factor. The main reason for this disappointing result, which however was considered likely in the experimental planning, resides in the difficulty of subtracting correctly the large incoherent intramolecular contribution from the coherent neutron diffraction data. In particular, one of the hard problems that we had to face was the lack of precise information on the incoherent cross section of para-hydrogen, for the large energy range that is relevant to a neutron diffraction experiment carried out at a pulsed source. In fact, using the data that were available in the literature, it was virtually impossible to work out a reliable correction procedure, due to the unfavourable ratio between the coherent and the incoherent cross section. On the other hand, a detailed knowledge of this quantity would allow us to develop an accurate model which, in the end, could possibly help in solving the problem of extracting the microscopic structure factor of light molecular hydrogen from the neutron diffraction experimental data.

To this end, we have planned a direct measurement of the neutron total cross section of molecular hydrogen, in the liquid phase, in the range of neutron energies that is available on a pulsed neutron source. In this paper we report on this experiment and we make some comparison with the results from the available theoretical models. In section 2 we give a detailed description of the experimental set-up. The analysis of the data and the extraction of the relevant experimental information is described in section 3. In section 4, we discuss the theoretical model and its comparison with the results. Finally, in section 5, we draw the conclusions of this work.

2. Description of the experiment

The experiment was carried out on the PEARL (Pressure and Engineering Advanced Research Line) beamline of the pulsed neutron source ISIS (UK). As the beamline is normally used for mechanical stress experiments, the local instrumentation was not suitable for our needs and we had to build a new pair of neutron detectors for a transmission experiment. In order to monitor the primary beam before and after it hits the sample, we used two thin vanadium foils. These had to be thick enough to give a relevant signal, but not so thick as to increase the expected neutron background. In addition, in order to reduce the effect of the presence of the vanadium foils on the sample, these were placed quite far apart from the sample container. We evaluated that, in our experimental geometry, the effect of the vanadium on the sample was smaller than 10^{-4}, i.e. well below the planned accuracy of the experiment.

The neutron detectors were made of lithium glass scintillators placed in closed contact with the window of the photomultipliers. The detectors (and the photomultipliers) were placed into a cylindrical well (wall thickness 10 cm) made of a boron-carbide-based resin (crispy mix) contained in an aluminium box. The well depth was much longer than the photomultiplier.

Therefore, only that portion of the vanadium foil that was hit by the neutron beam was visible by the detector.

In a transmission experiment, it is very important that the relative stability of the two monitors be very good over a long time period. To this end, we selected a pair of photomultipliers whose characteristics were very similar. Moreover, the relative stability of the two monitors was checked, on the timescale of several days, with satisfactory results. In particular, we found that the absolute stability of each monitor, taken separately, was of the order of 2% on a 24-hour timescale. However, since the measured drifts were probably due to temperature changes of the experimental hall, the measured relative stability of the two monitors turned out to be much better (of the order of 0.2%, on a 24-hour timescale). Also, we could safely use shorter sampling times, thus increasing the overall accuracy of our detection system.

The sample container was made of a flat cylindrical cell (diameter 55 mm, nominal thickness 2.5 mm), made of aluminium alloy, which was fixed to a copper thermal reservoir. This, in turn, was connected to the cold head of a liquid-helium cryostat. In addition, the sample container was connected with the external gas-handling system by means of a 1/16″ OD stainless steel tube, wrapped with an electric heater to avoid blockage. Inside the scattering cell, out of the neutron path, we had inserted a solid catalyst made of Cr_2O_3–γAl_2O_3, in order to increase the rate of conversion from ortho- to para-hydrogen.

The empty system was cooled down in the neutron beam and the reference transmission factor was measured. The relative distances between the sample and the vanadium foils, and between the vanadium and the detectors, were measured as accurately as possible using a meter. However, due to the difficult experimental conditions (the neutron path between the two vanadium foils was evacuated) we could only reach an accuracy of a few mm. A much better accuracy was obtained by inserting a thin uranium foil in the beam, upstream with respect to the sample, and using its resonances to calibrate the various distances [5].

Once the set-up was calibrated, and the reference transmission factor was measured, liquid hydrogen was condensed directly into the scattering cell. The temperature was set to $T = 16.0$ K and we set the pressure to $p = 0.3$ bar (the vapour pressure of hydrogen at this temperature is $p = 0.216$ bar) to make sure that the cell was full of liquid. The liquid sample was then subjected to small, rapid, temperature variations so that turbulence was induced that led to a continuous and efficient interaction with the catalyst. The rate of convergence was measured by observing the low-energy behaviour of the total neutron cross section. In fact, in the low-energy region, the scattering cross section of para-hydrogen is much lower than the corresponding cross section for normal hydrogen. Therefore, we could observe, in real time, the evolution of the sample towards thermodynamic equilibrium. Due the sample being thin, almost 20 hours were necessary to reach the thermodynamic equilibrium which, eventually, was obtained on the following day with an estimated composition of 99.96% of para-hydrogen.

As a final consideration, we point out that for each configuration we have carried out several runs of 5–6 hours in order to check the stability of the experimental set-up as well as the acquisition electronics. The overall stability of the sample, during the whole experiment, turned out to be very good, with a temperature stability within 0.2 K with respect to the set point, and an equivalent pressure oscillation in agreement with the equation of state of liquid para-hydrogen. The density of the sample, ρ, has been derived using reference [6].

3. Data analysis and results

As a first step, we have verified the stability of the spectra by comparing the different sub-runs. As the average differences turned out smaller that the statistical fluctuations, we could add the various sub-runs in order to reduce the statistical error. Then, we transformed the spectra from

the time of flight to the incident wavelength (or energy) using the results of the calibration measurement, according to the standard technique (see for example: reference [7]). We point out, in this context, that the background was measured, for both experimental configurations (empty and filled cell), leaving the incident neutron beam on and slightly turning the monitors so that the vanadium foils were not directly seen by the detectors. After subtracting the background, we obtained, for each experimental configuration, the ratio between the signals of the two monitors. This was in order to eliminate the effect of the intensity distribution of the incident neutron beam. Then, in order to eliminate the efficiency of the detectors, the scattering power of the vanadium foils, the attenuation of the aluminium can, and that of the first vanadium foil, we evaluated the ratio of these quantities. Finally, we were able to obtain the total cross section of liquid para-hydrogen from

$$\sigma(\lambda_0) = \frac{-1}{\rho t} \ln \left\{ \frac{(I_{S2} - B_{S2})}{(I_{S1} - B_{S1})} \frac{(I_{C1} - B_{C1})}{(I_{C2} - B_{C2})} \right\} \tag{1}$$

where I is the intensity measured from the vanadium monitor and B is its background. The subscripts S and C refer to the container filled with para-hydrogen and to the empty cell, respectively. The subscripts 1 and 2 refer to the monitor placed before (1) and after (2) the sample. The sample thickness, t, is a very important parameter for the data analysis. We used a value ($t = 2.66$ mm) that was determined, after completing the experiment, by averaging the measured distribution of the cell thickness (as a function of the displacement from the centre) with and without the same overpressure as in the experiment.

In figure 1 we show the typical raw data patterns for the transmission monitors. The higher spectrum is the reference pattern (empty cell), while the other is the one taken with

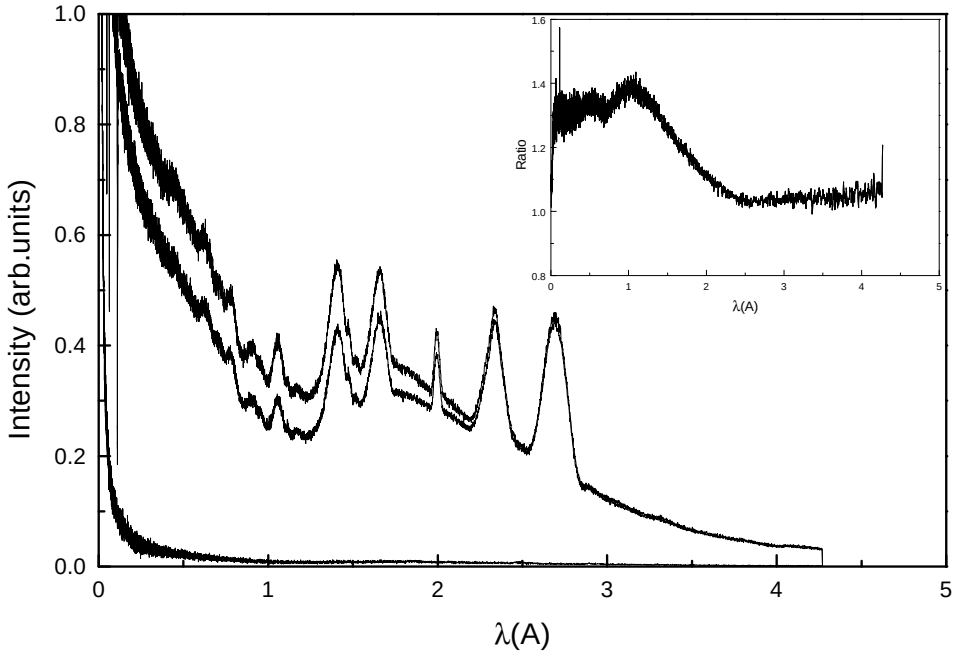

Figure 1. Raw data patterns taken on the transmission monitor. The higher spectrum is the reference pattern (empty cell) while the lower spectrum is obtained with the liquid para-hydrogen filling the sample container. The lowest pattern is the measured background. In the inset we show the ratio between the two spectra.

liquid para-hydrogen filling the sample container. Some Bragg peaks, originating from the various metal parts in the beam, are superimposed on the wavelength distribution of the incident neutron beam. The lowest pattern is the measured background. In the inset, we show the ratio between the two measured spectra showing the characteristic decrease of the para-hydrogen cross section in the long-wavelength region. The large decrease of the measured cross section at low energy is peculiar to para-hydrogen in the state $J = 0$. In fact, when the neutron energy is so small that no intramolecular transition is allowed, the para-hydrogen molecule behaves as a monatomic substance characterized by a scattering length that is simply given by the sum of the coherent scattering lengths of the two protons.

4. The theoretical model(s)

The Young and Koppel theory [8] models liquid hydrogen taking into account the spin correlations, rotations, and vibrations. These intramolecular modes are taken into account exactly, to the extent that vibration–rotation coupling can be neglected and that the vibrations can be considered harmonic. However, in the original work by Young and Koppel (YK), a perfect-gas model (no intermolecular interactions) was assumed for the translation dynamics. Within this approximation, the cross section is simply given by the molecular self-term; that is,

$$\begin{aligned}\frac{\mathrm{d}^2\sigma}{\mathrm{d}\Omega\,\mathrm{d}E_1} = {} & \frac{X^{(e)}}{Z^{(e)}} s^2_{ee}(i) \sum_{J=\text{even}} f(J) \sum_{J'=\text{even}} \sum_{v} \left(\frac{k_1}{k_0}\right) \left(\frac{M}{2\pi\, Q^2 k_B T \hbar^2}\right)^{1/2} \\ & \times \exp\left\{-\frac{M\,[\Delta E(J, J', v)]^2}{2\hbar^2 Q^2 k_B T}\right\} \\ & \times \frac{\alpha^{2v}}{4v!}(2J+1)(2J'+1) \sum_{L=\text{even}} (2L+1) \begin{pmatrix} J & J' & L \\ 0 & 0 & 0 \end{pmatrix}^2 |A_{Lv}(\alpha, \beta)|^2 \\ & + \frac{X^{(e)}}{Z^{(e)}} s^2_{eo}(i) \sum_{J=\text{even}} f(J) \sum_{J'=\text{odd}} \sum_{v} \left(\frac{k_1}{k_0}\right) \cdots \sum_{L=\text{odd}} (2L+1) \cdots \\ & + \frac{X^{(o)}}{Z^{(o)}} s^2_{oo}(i) \sum_{J=\text{odd}} f(J) \sum_{J'=\text{odd}} \sum_{v} \left(\frac{k_1}{k_0}\right) \cdots \sum_{L=\text{even}} (2L+1) \cdots \\ & + \frac{X^{(o)}}{Z^{(o)}} s^2_{oe}(i) \sum_{J=\text{odd}} f(J) \sum_{J'=\text{even}} \sum_{v} \left(\frac{k_1}{k_0}\right) \cdots \sum_{L=\text{odd}} (2L+1) \cdots . \end{aligned} \tag{2}$$

Here, k_0 and k_1 represent the momentum of the incident and scattered neutron, respectively, while Q is the momentum transfer. The initial vibrational state of the molecule is assumed to be $v = 0$ while $f(J)$ is the weight of the initial rotational state J. The final rotational and vibrational states are indicated by J' and v, while

$$\begin{pmatrix} \cdots & \cdots & \cdots \\ \cdots & \cdots & \cdots \end{pmatrix}$$

indicates the $3J$ symbol. The quantities $X^{(e)}$ and $X^{(o)}$ are the fractions of molecules in an *even* or an *odd* rotational state (e.g. pure para-hydrogen is characterized by $X^{(e)} = 1$ and $X^{(o)} = 0$). Also, $Z^{(e)}$ and $Z^{(o)}$ are the *even* and *odd* rotational partition functions. The four functions $s^2(i)$, where i is the nuclear spin, are combinations of the bound coherent and incoherent scattering lengths (a_{coh} and a_{inc}, respectively) of the nucleus and depend on the quantum statistics of the molecule. Their expressions for hydrogen are [9]

$$s^2_{ee}(H_2) = 4a^2_{coh} \tag{3}$$

$$s^2_{oo}(H_2) = 4a^2_{coh} + \frac{8}{3}a^2_{inc} \tag{4}$$

$$s^2_{eo}(H_2) = 4a^2_{inc} \tag{5}$$

$$s^2_{oe}(H_2) = \frac{4}{3}a^2_{inc}. \tag{6}$$

The function $A_{Lv}(\alpha, \beta)$ was introduced by YK and is defined as [9]

$$A_{L,v}(\alpha, \beta) = \int_{-1}^{+1} \mathrm{d}\eta \; P_L(\eta)\eta^v \exp\left\{-\frac{\alpha^2\eta^2}{2} + \mathrm{i}\beta\eta\right\} \tag{7}$$

where $P_L(\eta)$ is the Legendre polynomial of order L, $\alpha = Q(\hbar/2M\omega_v)^{1/2}$, and $\beta = (QD_e/2)$. Here, M, ω_v, and D_e are the molecular mass, the circular frequency of the intramolecular vibrational transition, and the equilibrium distance of the two nuclei, respectively. Finally, $\Delta E(J, J', v)$ represents the energy balance and is defined as

$$\Delta E(J, J', v) = [E_0 + E(J)] - \left[E_1 + E(v) + E(J') + \frac{Q^2\hbar^2}{2M}\right] \tag{8}$$

where E_0 and E_1 represent the energy of the incident and scattered neutron, respectively, and $E(J)$ and $E(v)$ are the rotational and vibrational energies. The last term represents the translational energy gained from the molecule.

Using the YK theory, and adding the small contribution coming from the absorption cross section, it is possible to evaluate the total neutron cross section for liquid para-hydrogen and the results are shown in figure 2. We point out that no fitting parameter has been used and that the comparison is carried out on an absolute scale. We observe that the model gives a rather good description, though qualitative, of the overall experimental cross section. However, it retains the relevant features of the cross section and should constitute a good reference point for a perturbation treatment. For example, it is interesting to observe that the rising edge of the cross section corresponds roughly to the first rotational transition ($J = 0$, $J' = 1$, $E_{\Delta J} = 14.5$ meV), while the energy corresponding to the vibrational transition is beyond the position of the second peak. Thus, the observed structure in the cross section is mainly due to the rotational structure of the molecules.

Even though the overall agreement observed in figure 2 is only qualitative, we observe that it becomes quantitatively relevant in the short-wavelength region (high-energy neutrons), especially in the region of energies beyond the first vibrational transition ($E_v = 0.545$ eV), where the intermolecular interactions are known to be less and less important. This is not unexpected, as the YK theory describes the hydrogens in the absence of interactions, i.e. in the condition of a very dilute gas phase. As the density increases, the effect of the intermolecular interactions increases too and the model is expected to fail, especially in the long-wavelength region.

In principle, the intermolecular interactions of hydrogen are composed of isotropic and anisotropic contributions. However, it is well known that the anisotropic contribution is negligible, as hydrogen, even in the condensed phases, behaves as an almost free rotor [10]. Therefore, it is a good approximation to assume that the intermolecular interactions are driven by a spherical potential. An even further simplifying assumption is to consider the effect of the free volume decreasing, as a function of density, from the ideal-gas limit to that of the dense liquid. Since hydrogen is a quantum fluid, the first effect of decreasing the free volume is an increase of the centre-of-mass kinetic energy according to the uncertainty principle $\delta r \, \delta p \geqslant \hbar$. This is a well known effect [11, 12] and we could use this result for improving the YK theory.

In a recent paper, we generalized the model taking into account only the isotropic component of the intermolecular potential [13]. In fact, by means of Path Integral Monte Carlo

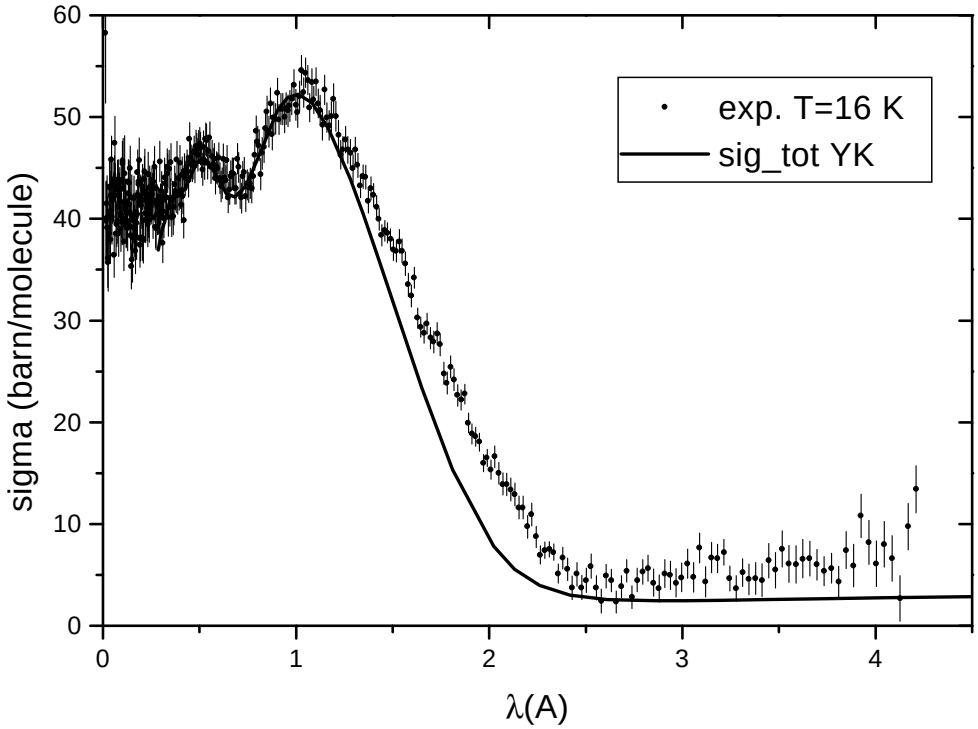

Figure 2. The total neutron cross section of liquid para-hydrogen at $T = 16$ K. Comparison between the experimental results and the YK theory. The agreement is only qualitative.

(PIMC) simulations, we are able to compute the effective kinetic energy of the molecular centre of mass of molecular hydrogen [14,15]. This value could be used to define an effective temperature, T_{eff}, according to the equation

$$\langle E_k \rangle = \frac{3}{2} k_B T_{eff}. \tag{9}$$

This effective temperature was used in the width of the translational Gaussian distribution in place of the true temperature (cf. equation (2)). In this way, we have defined a modified Young and Koppel (MYK) model which is expected to be more suitable for describing the liquid phase of para-hydrogen. In addition, to further improve the model, we used, for the vibrational and rotational levels, the measured correction terms that account for the centrifugal distortion and the anharmonicity corrections [13].

If we compare the experimental results obtained from the present experiment with the ones derived from the MYK model we arrive at the results that are depicted in figure 3. Obviously, as the MYK model does not take into account the details of the intermolecular interactions, the agreement is not perfect, especially in the intermediate region, where the intermolecular interactions are important and cannot be accounted for by simply renormalizing the kinetic energy of the molecular centre of mass. Nevertheless, with respect to figure 2, we observe that we have passed from a qualitative to a rather quantitative agreement, with the computed model crossing the experimental data at a few points. As was expected, no changes are observed in the short-wavelength region where the role of the intermolecular interactions is known to be less important.

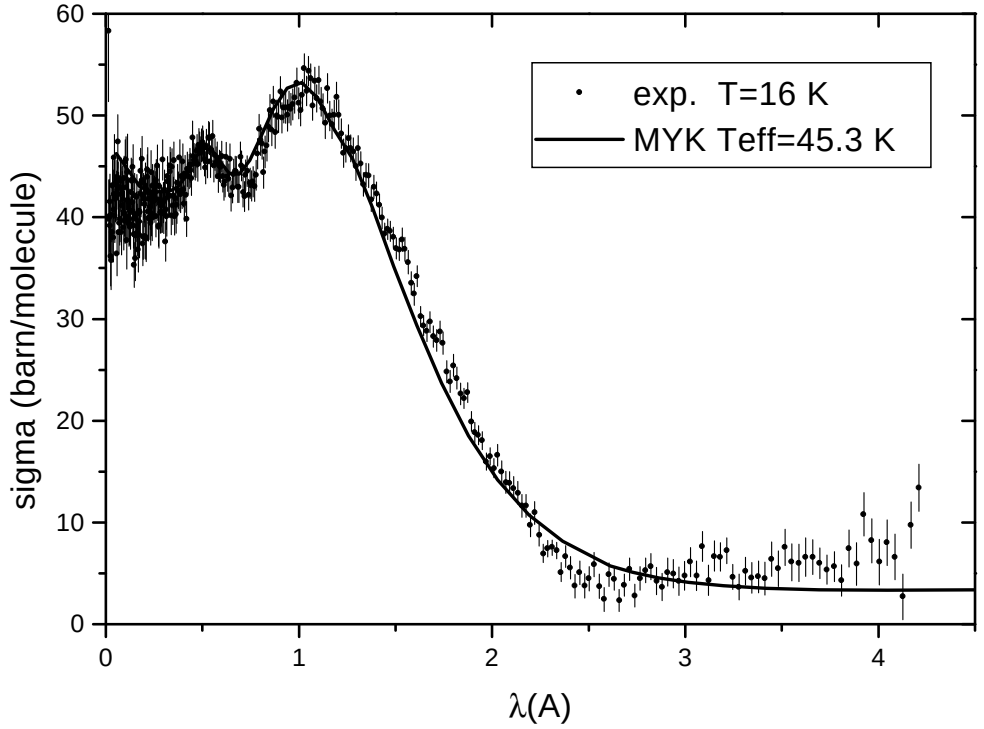

Figure 3. The total neutron cross section of liquid para-hydrogen at $T = 16$ K. Comparison between the experimental results and the MYK model. The overall agreement is improved and the theoretical results now cross the data at (at least) three points.

It is clear, from figure 3, that the intermediate region is affected by the details of the intermolecular interaction and therefore it cannot be quantitatively accounted for by our over-simplified model. Moreover, also the long-wavelength limit of the cross section does not seem to agree with the calculation results. In fact, the slight increase of the absorption cross section is not sufficient for the experimental behaviour to be recovered in the region $\lambda \geqslant 3$ Å. The measured increase of the cross section is explained, in the literature, as the effect of an increment of the apparent flux of the scattered neutrons that is determined by the transfer of the thermal energy from the target to the neutron (cf. reference [16]). This effect, however, is taken into account by the calculation. Therefore, the experimental data suggest that something else may play a role in producing the observed effect.

4.1. The low-energy limit

The YK theory is rather complex and is not possible, in general, to evaluate analytically the total cross section. However, this task becomes possible in the low-energy limit (LEL). The total cross section is obtained integrating equation (2) both over the final energy and the solid angle. That is,

$$\sigma(E_0) = \int_0^{2\pi} \mathrm{d}\phi \int_0^{\pi} \sin(\theta)\, \mathrm{d}\theta \int_0^{\infty} \mathrm{d}E_1\, \frac{\mathrm{d}^2\sigma}{\mathrm{d}\Omega\, \mathrm{d}E_1}. \tag{10}$$

For liquid para-hydrogen, when the energy of the incident neutron is so small that no intra-molecular transition can be excited, the double-differential cross section reduces drastically

(cf. equation (2)). First, only the $J = 0$ state is populated. Then, only the $J = 0 \rightarrow J = 0$ transition is allowed. Therefore, all the sums in equation (2) disappear and only the first term $s^2_{ee}(i)$ contributes to the cross section.

Thus, equation (10) can be worked out and, after some tedious but simple calculations, reduces to the LEL expression:

$$\sigma(E_0) = \frac{2s^2_{ee}(i)\sqrt{\epsilon\pi}}{(1+\gamma)^2} \int_0^{\pi} \sin(\theta)\, \mathrm{d}\theta \int_0^{\infty} \mathrm{d}q\, q \frac{\sin^2[qa(k_0)]}{[qa(k_0)]^2} \exp\{-b(E_0)q^2\} \times \exp\left\{-\epsilon\left[\cos^2(\theta) - q\cos(\theta) + \frac{q^2}{4}\right]\right\} \tag{11}$$

where: $\gamma = m/M$ is the ratio between the neutron mass m and the molecular mass M; θ is the scattering angle; $\epsilon = E_0/(\gamma k_B T)$ represents a normalized energy; and $q = Q(\gamma + 1)/k_0$ is a normalized momentum transfer. The quantities $a(k_0)$ and $b(E_0)$ contain the molecular parameters and are defined as

$$a(k_0) = \frac{k_0 D_e}{2(\gamma + 1)} \tag{12}$$

$$b(E_0) = \frac{E_0 \gamma}{E_v(\gamma + 1)} \tag{13}$$

where $E_v = \hbar\omega_v$ is the vibrational energy interval in the harmonic oscillator model of the isolated molecule. It is worthwhile to note that in the limit $D_e \rightarrow 0$, the molecular form factor in equation (11) tends to 1. In addition, when $E_0 \ll E_v$, the Debye–Waller factor also tends to 1 and the total cross section reduces to the expression for the monatomic ideal gas (the ideal-gas limit, IGL, corresponding to equation (3.167) of reference [16]).

For the sake of clarity we show, in figure 4, the comparison between the full numerical integration of equation (2) (full line) and its low-energy limit (LEL) represented by equation (11) (full squares). In the lower figure we report the YK model for para-hydrogen at

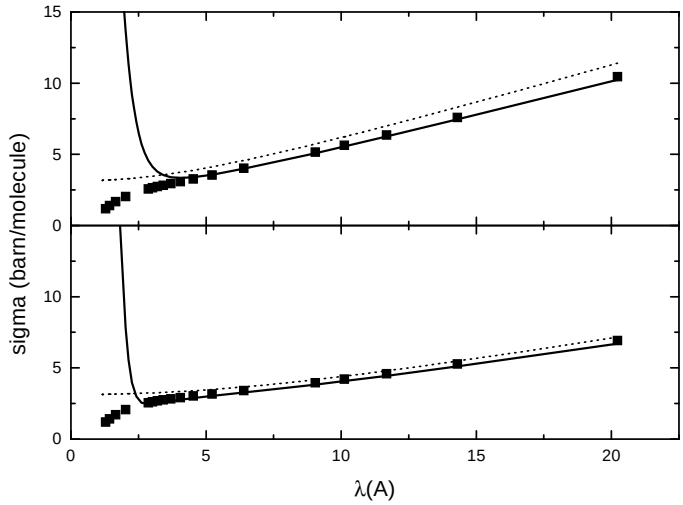

Figure 4. Comparison between the full numerical integration of equation (2) (full line) and its low-energy limit (LEL) given by equation (11) (full squares). The lower figure is related to the YK theory ($T = 16$ K) while the upper figure represents the MYK model ($T_{eff} = 45.3$ K). The dotted lines represent the ideal-gas limit (IGL).

$T = 16$ K as well as the LEL results evaluated at the same temperature. We see that the long-wavelength limit is respected. However, going to short wavelengths, the LEL cross section decreases to 0. This is due to the effect of the molecular form factors. Should we have used the molecular terms identically equal to 1 (the IGL), we would have obtained values converging to 3.13 barns per molecule (cf. the dotted line), i.e. the value that results from adding together the nuclear coherent scattering lengths of the two protons. However, the real situation is different for the molecular system. As the neutron wavelength decreases, the molecular cross section grows due to the effect of the intramolecular transitions (cf. the continuous line in the figure) and this overcompensates the decrease of the elastic coherent term. In the upper figure, we show the results from the MYK model. Here, the liquid para-hydrogen temperature is still 16 K. However, we used an effective temperature of 45.3 K. The change in the effective temperature results in a wider Gaussian factor in the expression for the cross section. The consequence is twofold. On one hand, the cross section rises faster than the crude YK model in the long-wavelength limit (a higher effective temperature increases the apparent flux of the scattered neutrons). On the other hand, in the short-wavelength region, the rise of the cross section due to the intramolecular transitions is smoother but starts at longer wavelengths.

We have shown that the theory accounts for an increase of the total cross section with λ but this is not sufficient for the long-wavelength discrepancy that is observed in both figures 2 and 3 to be recovered. Also, the small fraction of ortho-hydrogen still present as an impurity in the sample has a negligible effect with respect to the observed difference. Thus, some extra argument should be invoked. Here, we will use some very simple heuristic arguments to account for this behaviour.

In the region of the large λ, the velocity of the neutron decreases and the interaction time becomes so long that the scattering process is determined by the time integral of the interaction of the target molecule with its first-neighbour shell. In other words, we expect, at very long wavelength, the neutrons to feel a continuous distribution of particles and the target molecule to react with an *effective mass* that is *much larger* than the true molecular mass. In order to check this hypothesis, we have evaluated the total scattering cross section using the MYK model and testing the effect of the molecular mass on the behaviour of the total cross section. To this end, we have changed the molecular mass in the calculations and we have assumed that each hydrogen molecule is composed of two protons at a distance D_e apart, and a point mass of 24 amu placed at the centre of mass. This choice would take into account the fact that the neutron recoil should be determined not just by the single molecule, but also by its twelve nearest neighbours. The results of the calculation are reported in figure 5. Apart from in the low-wavelength region, where the calculation results rise too early, we see that the model is closer to the experimental data and that the correction imposed by this hypothesis significantly improves the agreement with the experimental results.

4.2. The high-energy limit

The high-energy limit of the calculations can be tested using the Fermi relation [17]:

$$\sigma_\infty = \sigma_{\text{bound}}\left(1 + \frac{m}{M/2}\right)^{-2} \tag{14}$$

where $M/2$ is the mass of the target atom. Alternatively, in order to check the behaviour of the cross section in a range of large but finite energies, one can evaluate, analytically, the high-energy limit of the YK theory. To this end it is necessary, first, to recast equation (8) as follows:

$$\Delta E(\Delta J, \Delta v) = \frac{\hbar^2 k_0^2}{2m} - \frac{\hbar^2 k_1^2}{2m} - E_{\Delta J} - E_{\Delta v} - \frac{\hbar^2 Q^2}{2M} \tag{15}$$

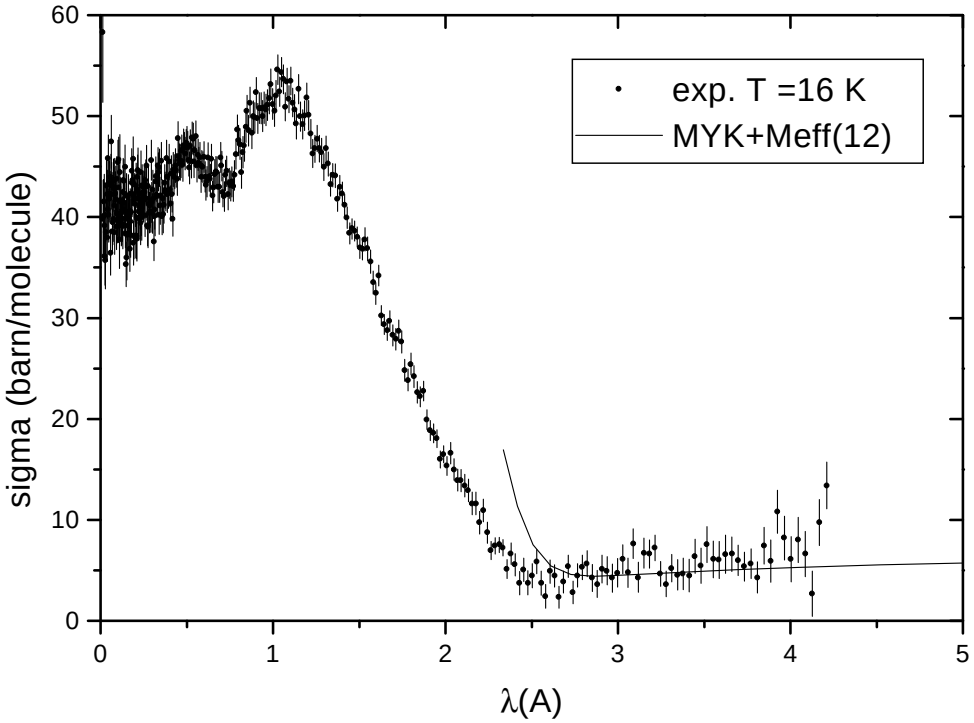

Figure 5. Comparison between the experimental results and the MYK model using a 26 amu effective mass. The model rises too early, decreasing λ, but the long-wavelength limit is now in better agreement with the experimental points.

where m is the neutron mass, and $E_{\Delta v}$ and $E_{\Delta J}$ represent the vibrational and rotational energy jumps, respectively. When the energy of the incident neutron becomes very large with respect to both $E_{\Delta v}$ and $E_{\Delta J}$, the intramolecular energy terms in equation (15) become negligible and their effect can be accounted for by assuming that the recoil mass, M, is substituted for with the *atomic* mass $M/2$ [13]. Therefore, equation (15) becomes simply

$$\Delta E = \frac{\hbar^2 k_0^2}{2m} - \frac{\hbar^2 k_1^2}{2m} - \frac{\hbar^2 Q^2}{M} = \frac{\hbar^2}{m}(\boldsymbol{k}_0 \cdot \boldsymbol{Q}) - \frac{\hbar^2 Q^2}{2m}(2\gamma + 1). \tag{16}$$

A direct consequence of equation (16) is that the Gaussian factor in equation (2) can be pulled out and, after some straightforward calculations, the equivalent of equation (10) becomes

$$\sigma(E_0) = \frac{\hbar^2}{mk_0}\int \frac{\mathrm{d}\boldsymbol{Q}}{Q}\left(\frac{M}{2\pi k_B T\hbar^2}\right)^{1/2} \exp\left[-\frac{M\Delta E^2}{2Q^2\hbar^2 k_B T}\right] v(Q,0). \tag{17}$$

The function $v(Q,t)$ has been introduced in reference [9]. However, here we need only the $t = 0$ value of this function, which, for low-temperature liquid hydrogen, becomes simply [9]

$$\begin{aligned} v(Q,0) &= 2(a_{coh}^2 + a_{inc}^2) + 2\left\{a_{coh}^2 - a_{inc}^2\left[1 - \frac{4}{3}X^{(o)}\right]\right\} I(\alpha\sqrt{2}, 2\beta) \\ &\simeq 2(a_{coh}^2 + a_{inc}^2) + 2\left\{a_{coh}^2 - a_{inc}^2\left[1 - \frac{4}{3}X^{(o)}\right]\right\} \exp(-2\alpha^2)\frac{\sin(2\beta)}{\beta}. \end{aligned} \tag{18}$$

Substituting equation (18) into equation (17), it turns out that the total cross section is given by a sum of two contributions:

$$\sigma(E_0) = \sigma_1(E_0) + \sigma_2(E_0). \tag{19}$$

The first term, $\sigma_1(E_0)$, has a structure similar to that of an ideal gas and therefore can be evaluated immediately (see, for example, section 3.7 of reference [16]). The result is

$$\sigma_1(E_0) = 4\pi \frac{2(a_{coh}^2 + a_{inc}^2)}{(1+\gamma)^2} \left\{ \Phi(\sqrt{\epsilon}) \left(1 + \frac{1}{2\epsilon} \right) + \frac{1}{\sqrt{\pi\epsilon}} \exp(-\epsilon) \right\} \tag{20}$$

where $\Phi(x)$ is the error function of real argument x.

The second contribution, $\sigma_2(E_0)$, is more involved. However, the 3D integral can still be reduced, after some tedious but straightforward calculations, to a 1D integral over a finite interval [18]. The result is

$$\sigma_2(E_0) = 2(a_{coh}^2 - a_{inc}^2) \frac{\gamma}{k_0 D_e} \sqrt{\frac{\epsilon}{\pi}} I_2(E_0) \tag{21}$$

where $I_2(E_0)$ is defined as

$$I_2(E_0) = 2\pi \frac{\sqrt{\pi}}{b} \int_0^1 \mathrm{d}x \ \exp(-\epsilon\gamma^2 x^2) \, \mathrm{Im}[w(z) + w(z^*)] \tag{22}$$

and $w(z) = \exp(-z^2)[1 - \Phi(-\mathrm{i}z)]$ is the error function of complex argument [19], with $z = (-\mathrm{i}ax + c)/b$ and the real constants a, b, and c, defined as

$$a = \epsilon\gamma^2(\gamma + 1) \tag{23}$$

$$b = \sqrt{64(E_0/E_v) + \epsilon\gamma^2(\gamma+1)^2} \tag{24}$$

$$c = k_0 D_e. \tag{25}$$

The numerical integration of equation (22) is trivial and the results are reported in figure 6, together with the measured cross section and the results from the MYK model.

We observe that the analytical calculation (in the high-energy limit) agrees with the experimental results in the region beyond 1 eV, while the result for the MYK model seems to diverge at high energy. This is probably due to numerical problems that affect the evaluation of the model when many rotational and vibrational levels have to be included in the calculations.

5. Conclusions

The total neutron cross section of liquid para-hydrogen is affected both by intramolecular and intermolecular features. The intramolecular features can be accounted for almost exactly using the YK theory. This is a molecular model where the spin correlations, rotations, and vibrations are taken into account exactly, to the extent that vibration–rotation coupling can be neglected and that the vibrations can be considered harmonic. However, the YK theory does not account for the intermolecular interactions. An oversimplified way of taking the intermolecular interactions effectively into account can be found using the MYK model, where the kinetic energy of the molecular centre of mass is renormalized using the results of the PIMC simulations of liquid para-hydrogen. In this way we observe a significant improvement of the agreement between the measured and the computed total neutron cross section (cf. figure 3). However, some differences still remain in the intermediate region of λ, which extend also to the long-wavelength regime. Improving the agreement in the intermediate region of λ is rather difficult, as it is necessary to evaluate the details of the intermolecular interactions, and therefore microscopic structural information is needed. Dealing with the long-wavelength

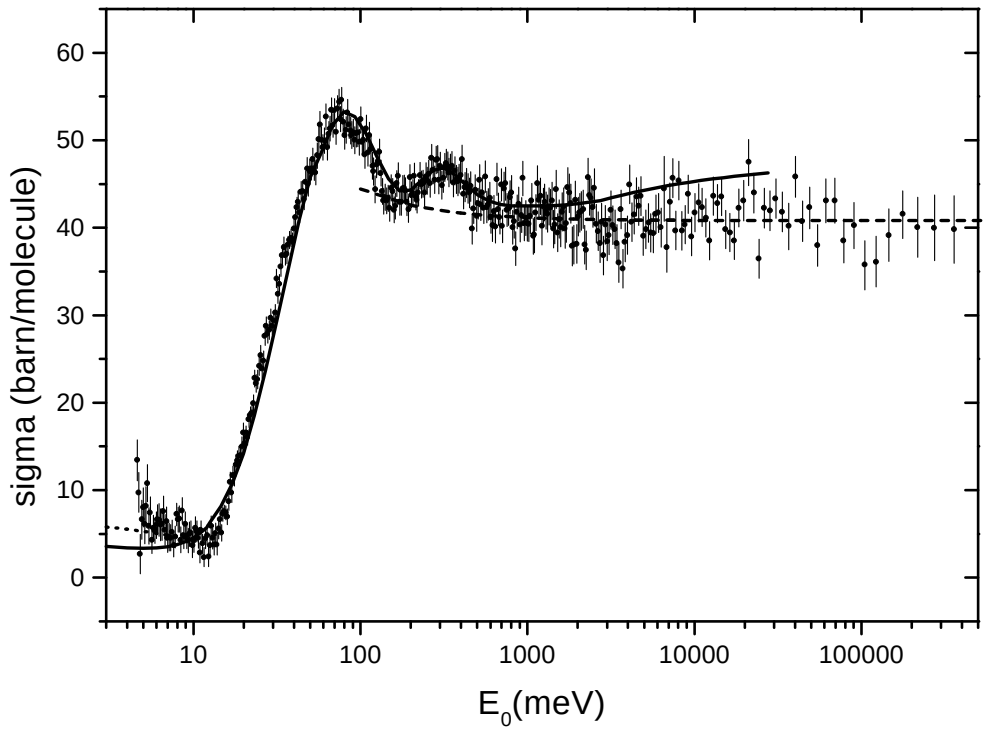

Figure 6. The total neutron cross section of liquid para-hydrogen ($T = 16$ K) as a function of the incident energy. Comparison between the experimental results and the various models. The MYK model is represented by the full line. In the low-energy region we use a heuristic effective mass of 26 amu (dotted line).The dashed line represents the high-energy limit of the YK theory that has been solved analytically. The overall agreement is very good and covers the whole energy range.

region, instead, appears less demanding. In fact, a simple increase of the molecular effective mass seems to improve the agreement in this region quantitatively.

Even though the inclusion of an effective mass improves the agreement between the experiment and the calculation to a semi-quantitative level, it seems that a larger effective mass would be necessary to make it better. However, the inclusion of more neighbours in the effective-mass model does not seem realistic. Therefore, we are led to conclude that some effect should also be attributed to the zero-point motion of the intramolecular vibrational mode which provides a kinetic energy reservoir for the two protons. This is an interesting hypothesis, but to exploit it to its full extent exceeds the scope of the present work.

As regards the high-energy limit, the model seems to suffer when many rotational and vibrational levels are included in the calculation (i.e. beyond 1–2 eV). However, in this case, we could obtain much better results by evaluating, analytically, the high-energy limit of the model.

In conclusion, we have shown that, using very simple heuristic arguments, a semi-quantitative description of the total neutron cross section of liquid para-hydrogen can be obtained over a very wide energy range. From the results reported in figure 6, we observe that the model describes quite well the total cross section of liquid para-hydrogen over the whole energy interval beyond 5 meV—that is, the energy range generally used in a spallation neutron source experiment. We are confident that this information will help us in extracting

microscopic structural information from the large incoherent background that is present in the diffraction data for liquid para-hydrogen.

References

[1] Balucani U and Zoppi M 1994 *Dynamics of the Liquid State* (Oxford: Oxford University Press)
[2] Poll J D and Miller M S 1971 *J. Chem. Phys.* **54** 2673
[3] Ceperley D M 1995 *Rev. Mod. Phys.* **67** 279
[4] Zoppi M, Celli M and Soper A K 1998 *Phys. Rev.* B **58** 11 905
[5] Mayers J and Evans A C 1991 *Rutherford Appleton Laboratory Report* RAL-91-048
[6] Roder H M, Childs G E, McCarty R D and Angerhofer P E 1973 *NBS Technical Note* No 641
[7] Windsor C G 1981 *Pulsed Neutron Scattering* (London: Taylor and Francis)
[8] Young J A and Koppel J U 1964 *Phys. Rev.* A **33** 603
[9] Zoppi M 1993 *Physica* B **183** 235
[10] Van Kranendonk J 1983 *Solid Hydrogen* (New York: Plenum)
[11] Langel W, Price D L, Simmons R O and Sokol P E 1988 *Phys. Rev.* B **38** 11 275
[12] Herwig K W, Gavilano J L, Schmidt M C and Simmons R O 1990 *Phys. Rev.* B **41** 96
[13] Bafile U, Celli M and Zoppi M 1996 *Physica* B **226** 304
[14] Zoppi M and Neumann M 1991 *Phys. Rev.* B **43** 10 242
[15] Zoppi M and Neumann M 1992 *Physica* B **180+181** 825
[16] Lovesey S W 1987 *Theory of Neutron Scattering from Condensed Matter* vol 1 (Oxford: Oxford University Press)
[17] Fermi E 1936 *Ric. Sci.* **7** 13
[18] Zoppi M 1999 unpublished
[19] *Handbook of Mathematical Functions* 1965 ed M Abramovitz and I A Stegun (New York: Dover)